Supplementary Results:

Epidermal growth factor receptor subunit locations determined in hydrated cells with environmental scanning electron microscopy

Diana B. Peckys, Jean-Pierre Baudoin, Magdalena Eder, Ulf Werner & Niels de Jonge

1. Testing for the presence of a water layer on a cell

The images from the gaseous secondary electron (GSE) detector were used to evaluate the presence of the water layer on the cell surface during imaging with environmental scanning electron microscopy (ESEM). A water layer was assumed to cover the cell surface if the same gold nanoparticles (AuNPs) were clearly visible in the image recorded with the scanning electron microscopy (STEM) detector but only barely or not visible in the GSE image. **Supplementary Fig. S1a-c** show the increasing contrast obtained on the labels from the GSE signal for decreasing pressure and thus reducing thickness of the water layer, compared to simultaneously recorded STEM images (**Supplementary Fig. S1d-f**). The images **Supplementary Fig. S1a** and **d** were taken at a pressure of 740 Pa, slightly above the pressure value[1] that will allow for condensation of water vapor at a temperature of 3 °C. Whereas the Au-labels are clearly visible in the STEM image, they can only barely be recognized in the GSE image. This can be explained by the obstructing effect that a water layer of a certain thickness has on the exit of electrons originating from the underlying Au-labels. The water layer retracted after lowering the chamber pressure to 700 Pa, thus moving the water/vapor equilibrium towards the threshold for water evaporation. Indeed, more labels are visible in **Supplementary Fig. S1b**. Reducing the pressure to 680 Pa further increased the number of visible AuNPs as shown in **Supplementary Fig. S1c**. The contrast in the STEM images **Supplementary Fig. S1d-f** was not notably affected by these pressure changes.

The GSE signal mainly derives from secondary electrons originating from a restricted depth of the sample. The maximum depth from which electrons can escape from a material is about 5 times[1] the mean free path length (λ) of the electron[2]. For an electron energy of 30 kV, λ

equals approximately 0.06 μm in water, resulting in a theoretical maximum water thickness of about 0.3 μm through which signals originating from AuNP labels can be detected with the GSE. A fading of the Au-label visibility would thus indicate a water layer that approaches this thickness.

To quantify the AuNP visibility, the signal-to-noise-ratio (SNR) was calculated from line scans drawn over the AuNPs in GSE images recorded of each pressure (**Supplementary Fig. S1**), four line scans on AuNPs in GSE images were analyzed resulting in SNR values of 1.7 ± 0.4 (the error margin reflects the standard deviation) at 740 Pa, 2.0 ± 0.3 at 700 Pa and 2.9 ± 0.6 at 680 Pa. For comparison, similar Au-label line scans in the dark field STEM images resulted in SNR values of 11 ± 2. This measurement confirms the effect of the water layer on the signals from both detectors.

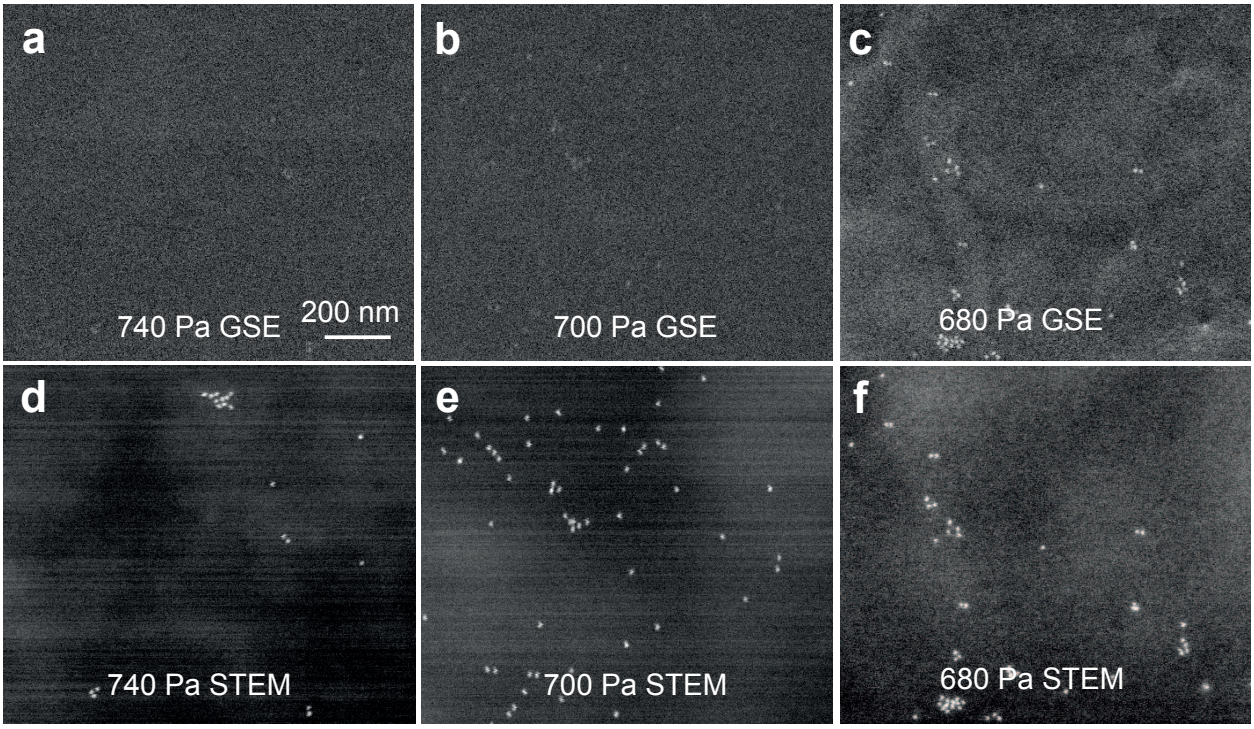

Supplementary Fig. S1. Verification of the presence of a water layer on an A547 cell during ESEM. (**a-c**) Images recorded with the GSE detector at three comparable thin regions of the cell for different pressures. (**d-f**) STEM images recorded simultaneously with the images a-c. Sample and settings as described in the methods of the main text.

2. The spatial resolution of ESEM-STEM

The spatial resolution obtained on the AuNP labels with ESEM-STEM was measured from line-scans (signal versus position) over selected labels (**Supplementary Fig. S2a**). As measure of the resolution we used the 25-75% edge width ($r_{25\text{-}75}$) of the signal peak over the AuNP (**Supplementary Fig. S2b**). This measure provides an upper value of the resolution and is valid for the case that the size of the nanoparticle is larger than the focused electron probe[3]. Line scans were drawn over a total of 12 AuNPs in 8 images for both COS7 and A549 cell types. The averaged $r_{25\text{-}75}$ resulted in 3.4 ± 0.7 nm. The spatial resolution obtained on the AuNPs with ESEM-STEM was thus 3 nm.

That the $r_{25\text{-}75}$ is a correct measure of the resolution was confirmed by determining the size of AuNPs. The measured full width half maximum (FWHM) of the signal peaks over the above mentioned AuNPs indicated a mean size of 11 ± 1 nm. The size of this type of AuNPs (from the same batch) was also measured via transmission electron microscopy from a dry test sample without cellular material, and its value of 12 ± 1 nm (from 28 AuNPs) was in good agreement with the value from the ESEM images. Since the size of the AuNP was not notably broadened in the wet ESEM images, for example, by electron scattering of the beam in the sample, it is reasonably to assume that the electron probe was smaller than the AuNP size.

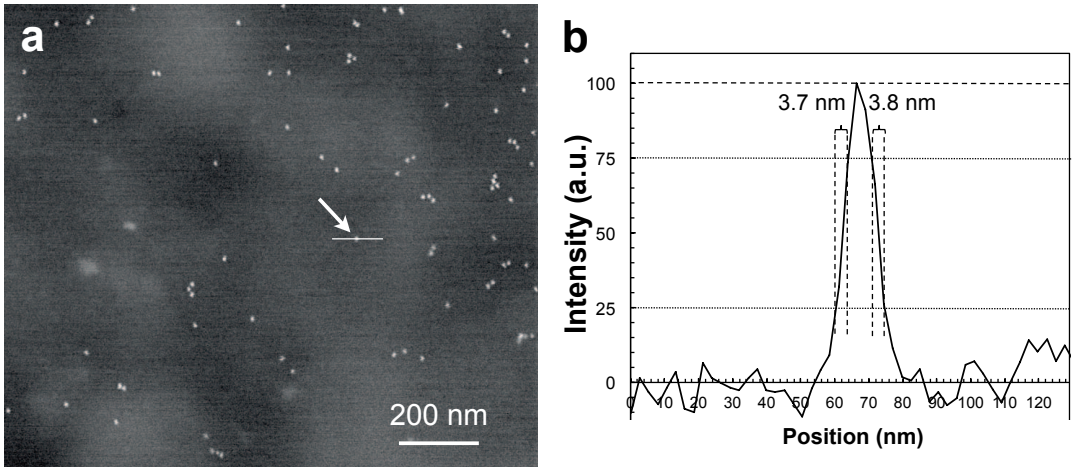

Supplementary Fig. S2. Measuring the spatial resolution of ESEM-STEM. (**a**) Dark field ESEM-STEM image of EGF AuNP labels on an A549 cell. The magnification was 50,000×, the pixel size was 2.7 nm, the temperature was 3 °C, and the pressure was 740 Pa. Sample and further settings as described in the methods of the main text. (**b**) Line scan drawn over the AuNP at the labeled position in **a**. The signal peak of the line scan reveals an 25-75% edge width $r_{25\text{-}75}$ of 3.7 and 3.8 nm for the left and right side, respectively.

3. Testing the labeling specificity

A control experiment was performed in parallel to the labeling experiments to test the specificity of the binding of the EGF-AuNP to the EFGR. The experimental protocols were repeated exactly as described in the online methods, except that no biotinylated EGF was added to the streptavidin AuNPs. The labels thus consisted of washed (=freed from unbound streptavidin) streptavidin conjugated AuNPs. The control experiment shows a low density of non-specifically bound single labels (**Supplementary Fig. S3**). Note that the brightness of the cellular material in the image may differ between figures on account of the brightness and contrast settings. Dimers and clusters are absent. Eight images, covering of a total area of 165 μm^2 on 5 different cells, included 125 AuNPs only. The average density of strept-AuNPs was 0.7 ± 0.3 / μm^2, while the average density of EGF-AuNPs was 13 / μm^2 on COS7 cells and 9 / μm^2 on A549 cells.

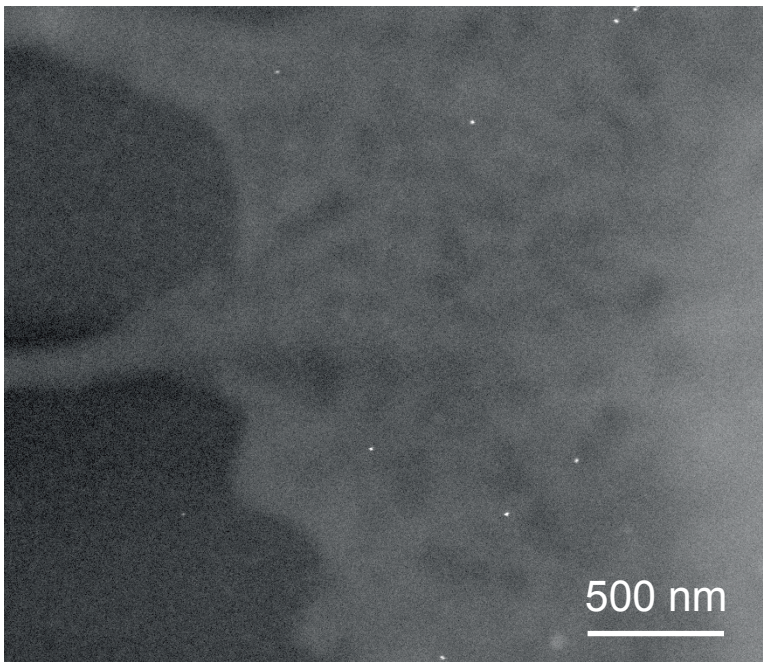

Supplementary Fig. S3. ESEM image of a region of a COS7 cell incubated with AuNP labels without EGF. Sample and settings as described in the methods of the main text.

4. Measurement of the effect of electron beam irradiation

To assess a potential impact of radiation damage on the distribution and the spatial organization of the labeled EGFRs, 19 regions of four different A549 cells with Au-labeled EGFRs were imaged twice at a range of electron doses distributed between 0.5 and 7.5 e^-/nm^2 in total for the image pair. An example is shown in **Supplementary Fig. S4**. Since the dose limit[4] used for cryo TEM studies of cells amounts to ~1 e^-/nm^2, we assumed that half this dose would represent a reasonable lower limit of the allowed dose for ESEM of fixed hydrated cells. An image pair recorded with a dose below the radiation damage limit would thus show no differences between the imaged features, i.e, the positions of AuNPs would be conserved. Each pair of images was aligned to correct for, e.g., possible stage drift, and an overlay image was created (ImageJ, NIH). These images were then analyzed for the shifts of the AuNPs. It was observed that the positions were conserved for all used doses for most of the area imaged. Nevertheless measurable shifts occurred mainly at the top and bottom edges of the images. The average shift of all AuNPs in these images, 1332 in total, amounted to 8 nm with a standard deviation of 11 nm. The maximal shift found for one AuNP in one image was 58 nm. But it should be noted that some membrane regions might include membrane ruffles representing flexible structures. There was no trend with the electron dose. The shifts occurred in a preferential direction indicating sample shrinkage. The maximal shrinkage relative to the image size was calculated as (8+11) nm / 884 × 2.7 nm < 1%, for an image with a pixel size of 2.7 nm. The samples were thus not entirely devoid of radiation damage but the damage was of such small degree that it was deemed acceptable.

To verify that radiation damage did not significantly influence the measured dimer distances, we recorded image pairs in 12 regions of 4 cells, with 10 different electron doses between 0.5 and 7.5 e^-/nm^2 total for the image pair. The dimers in these image pairs were selected (two AuNPs labels placed within 29 nm of center-to-center distance), the AuNP distance within each dimer was determined for the image pair, and for each dimer, the difference in the label distance between both images was calculated (for many a difference did not occur). A total of 227 dimer distances was determined for the 10 different electron doses. The average difference in distance for each dose was smaller than 1.2 nm. The maximal difference found for one dimer was 3 nm. Since the pixel size of the images was 2.7 nm, limiting the precision of the distance measurements, it can be concluded that there was no significant effect of the electron dose on the measured dimer distance. To test for a possible effect of radiation damage on the pair correlation

function, we also checked for the occurrence of differences in the measured distances in AuNPs larger than those of dimers in a range of up to 300 nm. A total of 37 distances was measured in three image pairs with doses of 0.5, 3.6, and 7.5 e^-/nm^2, and the average difference amounted to 1.0 nm. Thus, electron beam irradiation did not significantly influence AuNP distances in the range measured by the pair correlation function.

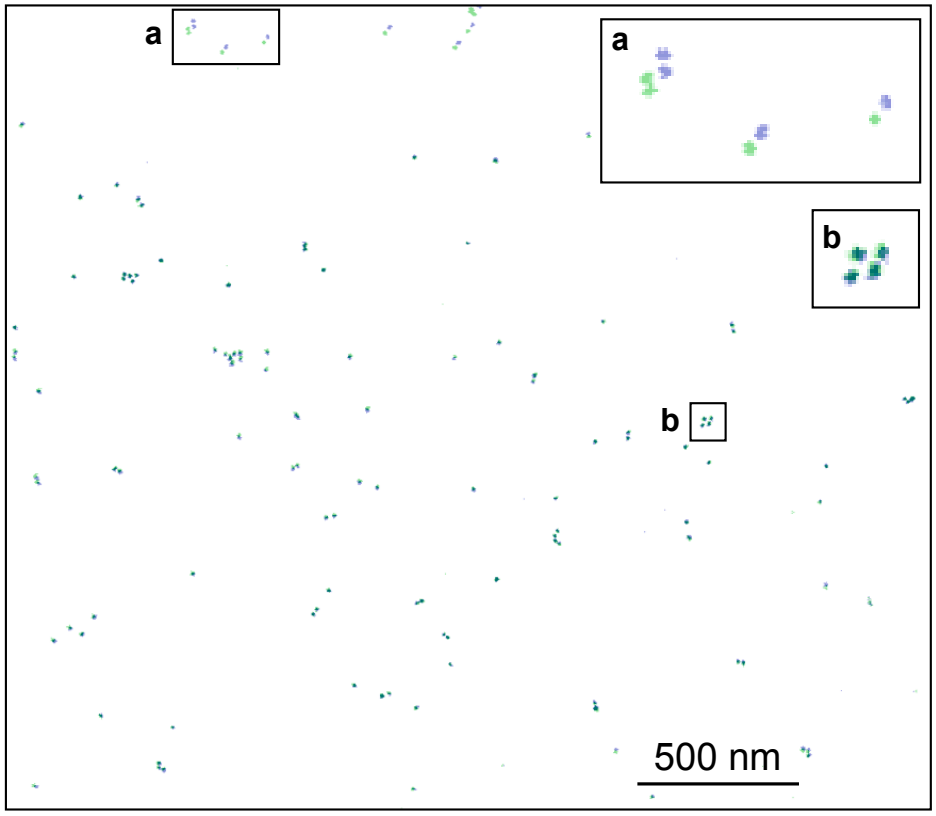

Supplementary Fig. S4. Overlay image generated from two subsequently recorded ESEM images of labeled EGFRs on an A549 cell as test of radiation damage. The image pair was recorded with a total dose of 4.2 e^-/nm^2. The magnification was 44,000×, and the pixel dwell time was 50 μs. The applied image processing (with ImageJ) included background subtraction, thresholding and color-coding of the bound EGF-AuNP labels, blue for the first, and green for the second image. Both images were then superposed, and aligned for stage drift. The overlay image shows that some labels in the upper image region had shifted, while the majority of labels remained at their respective locations. Enlarged details from the upper region (a), and from a region without shift (b) depict that, regardless of a detectable shift, the measured inter-pair distances of labeled EGFR dimers were not affected by the radiation dose.

5. Image processing

For the determination of particle positions, an image-processing algorithm on the basis of a macro command interpreter was implemented (written in GFA-Basic 32 for Windows). The image processing procedure is exemplarily shown for the bright field ESEM-STEM image shown in (**Supplementary Fig. S5a**). The first step was the minimization of filtering artifacts at the edge regions of the images. This was done by enlarging the image through mirroring the interior regions at the edges to the outside. Next followed Gaussian low-pass filtering, and the subtraction of the resulting smoothed filtered image from the original one eliminated the deep space frequencies (**Supplementary Fig. S5b**). The accurate and effective achievement of this filtering step was an essential condition for a successful data analysis, because only the precise elimination of deep spatial frequencies allowed a nearly artifact-free separation of the single particle images from the image, and with this the accurate determination of their positions in case of unfavorable contrast conditions. A few images displayed small horizontal stripes, created by interferences in the DF segment of the STEM detector. These were suppressed with the FFT bandpass filter operation implemented in ImageJ (NIH, USA). The following step was the elimination of the spatial frequencies above the fundamental frequency by Gaussian filtering to remove noise. Since the image background still varied due to inhomogeneous contrast generated by cellular material in the environment of the particles, a local acting binarization procedure was used as next step, which was controlled only by the intensities in the neighborhood of the particles. Single pixels caused by noise were removed from the binary image by using hit-miss operations.

The particle coordinates were found from the binary particle images, representing the vertical projections of the particles, by calculating the gravity centers of the projection areas. At the end of the image processing, circles were drawn into the original image at the captured particle positions (**Supplementary Fig. S5c**), thus allowing a visual estimation of the errors in the particle position measurements. For 96% of the particles, their positions were determined with a precision better than the pixel size. The automated procedure did not function for 4% of the particles. The majority of these 4% resulted from particles of a too low contrast preventing their detection, while several other particles were in clusters and inseparable in contrast. The 4% with erroneous detection did not lead to errors in the particles analysis. Next, the result of applying a density-based spatial clustering algorithm[5] was converted into a red labeling of

clustered particles and the drawing of circles around the identified clusters, as shown in **Supplementary Fig. S5d**.

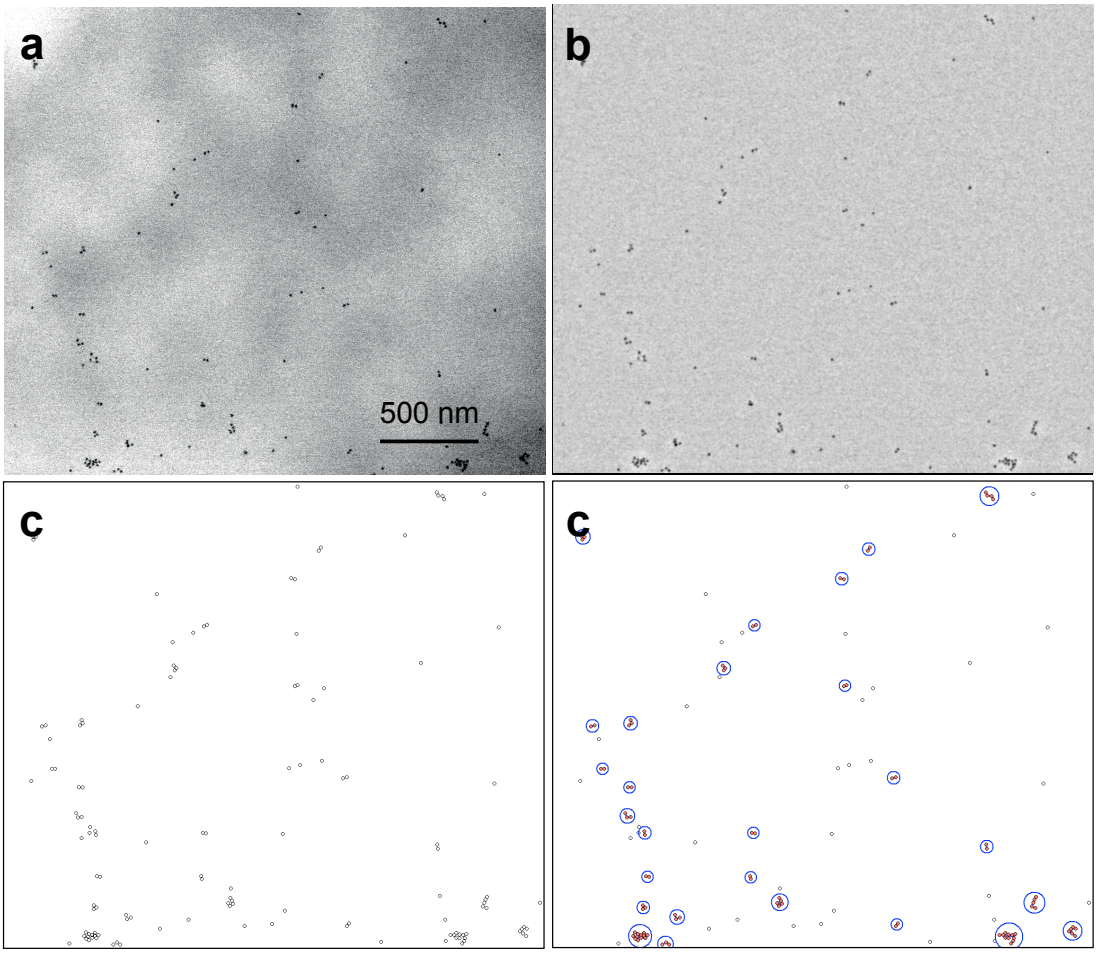

Supplementary Fig. S5. Image processing of ESEM-STEM images. (**a**) Example of an original bright field ESEM-STEM image of EGF-AuNPs on COS7 cells. (**b**) Filtered image of the particles with the low frequency information removed. (**c**) Automatically determined particle positions marked by circles. (**d**) Visual representation of the cluster analysis of the 129 imaged particles found in this image. Blue circles were drawn around particles that were not monodispersed (marked with red). The image included 15 particle pairs, 10 clusters with 3 to 5 particles, and 3 clusters with more than 5 particles.

6. Membrane sheets with AuNP labeled EGFRs

To compare the spatial dimensions of labeled EGFR dimers on whole cells obtained with ESEM with results obtained with an existing method, we prepared membrane sheets from A549 cells, and labeled EGFRs with the same EGF-Au-labels as used on the whole cells. ESEM analysis revealed similar Au-label distributions as found on whole cells imaged in hydrated state with ESEM, i.e. mono-dispersed AuNPs, pairs, and small clusters (**Supplementary Fig. S6a, b**). The pair distance was measured from the peak positions in a line scan (**Supplementary Fig. S6c**), and amounted to 19 nm. From the analysis of 62 pairs it was found that the dimer distance measured 19 ± 4 nm (**Supplementary Fig. S6d**) consistent with the findings in the main text.

The membrane sheets were prepared according to published protocols[6, 7]. In short, 80% confluent A549 cells were seeded to a final density of 1.0 x 10^5 cells/mL on glass cover slips and cultivated for 1 day with Dulbecco's Modified Eagle Media **(**DMEM), supplemented with 10% fetal bovine serum, at 37 °C and 9% CO_2. Cover slips with attached cells at a confluency of ~80% were incubated in 25 µL 4.5 nM EGF-AuNP labeling solution for 5 min at 37 °C. After two washing steps in Phosphate Buffered Saline (PBS), cover slips were pre-fixed in 1% freshly prepared, and pre-warmed paraformaldehyde for 10 min at 37 °C, and then rinsed again in PBS. Formvar-coated copper TEM grids were coated with 0.1% poly-L-lysine (PPL) for 10 min. A cellulose acetate filter disk was attached on a petri dish with 200 µL of PBS, and TEM grids were placed on the filter with the formvar and PLL coated side upwards. A cover slip was then placed on the grids with the cells facing the grids. Using a cork the cover slip was pressed down on the grids for 5 to 7 seconds. After 30 seconds, the cover slip was lifted, TEM-grids were collected, rinsed 3 times in 30 µL droplets of ice-cold PBS, and then fixed in 2% glutaraldehyde in PBS for 15 min at room temperature. The following fixation and washing steps of the membrane sheets mounted on TEM grids were performed in 30 µL droplets. Grids were washed twice in PBS followed by incubation in glycine-PBS for 3 min, and two washing steps each, first in PBS, and then in 0.1 M sodium cacodylate buffer, pH 7.4 (CB). The TEM grids were post-fixed in 1% OsO_4 in 0.1 M CB for 20 min at room temperature, washed twice in 0.1 M CB, and incubated in 1% tannic acid dissolved in HPLC grade water (HPLC-H_2O) for 10 min, followed by 4 washing steps in HPLC-H_2O. TEM grids were air dried on filter paper, and stored on a TEM grid pad until imaging in the ESEM (within 3 days after preparation).

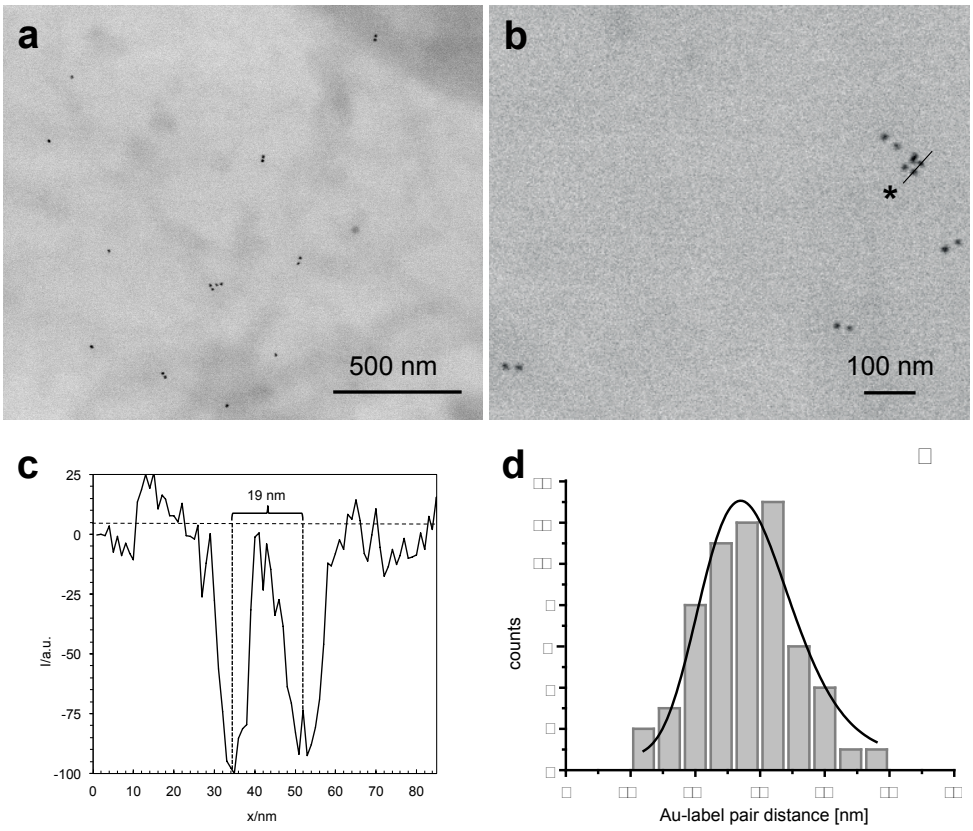

Supplementary Fig. S6. AuNP labeling of EGFRs in membrane sheets prepared from A549 cells. (**a**) Bright field ESEM overview image of EGFRs labeled in fixed membrane sheets with the same EGF-AuNP-labels. The image was acquired at 50,000 × magnification, an image size of 1024 × 884 pixels, a pixel size of 2.7 nm, pressure of 400 Pa, a temperature of 18 °C (sample inserted without pumping cycles), and with 30 kV acceleration voltage. (**b**) Image recorded at a magnification of 126,000 x, an image size of 2048 x 1868 pixels, and a pixel size of 1.1 nm. (c) Measurements of inter-pair distance via line scan line labeled * in panel **b**. (**d**) Dimer distance distribution histogram and the corresponding Log-normal fit derived from 62 similar line plots over double-labeled EGFR dimers, in 5 images.

Supplementary References

1. Stokes, D.J. Principles and Practice of Variable Pressure/Environmental Scanning Electron Microscopy (VP-ESEM), Edn. 1. (John Wiley & Sons Ltd, Chichester, UK; 2008).
2. Royall, C.P., Thiel, B.L. & Donald, A.M. Radiation damage of water in environmental scanning electron microscopy. *J. Microsc.* **204**, 185-195 (2001).
3. Reimer, L. & Kohl, H. Transmission electron microscopy: physics of image formation. (Springer, New York; 2008).
4. Hoenger, A. & Bouchet-Marquis, C. Cellular tomography. *Adv. Protein Chem. Struct. Biol.* **82**, 67-90 (2011).
5. Ester, M., Kriegel, H.-P., Sander, J. & Xu, X. in Second International Conference on Knowledge Discovery and Data Mining 226-231 (AAAI Press, 1996).
6. Hancock, J.F. & Prior, I.A. Electron microscopic imaging of Ras signaling domains. *Methods* **37**, 165-172 (2005).
7. Lillemeier, B.F., Pfeiffer, J.R., Surviladze, Z., Wilson, B.S. & Davis, M.M. Plasma membrane-associated proteins are clustered into islands attached to the cytoskeleton. *Proc Natl Acad Sci* **103**, 18992-18997 (2006).